Available online at www.sciencedirect.com
SCIENCE DIRECT®
Journal of Solid State Chemistry 178 (2005) 3541–3546
JOURNAL OF SOLID STATE CHEMISTRY
www.elsevier.com/locate/jssc

Preparation and thermal expansion of $\left(M^{III}_{0.5}M'^{V}_{0.5}\right)P_2O_7$ with the cubic ZrP_2O_7 structure

Tamas Varga[a], Angus P. Wilkinson[a,*], Michael S. Haluska[b], E. Andrew Payzant[c]

[a]School of Chemistry and Biochemistry, Georgia Institute of Technology, Atlanta, GA, 30332-0400, USA
[b]School of Materials Science and Engineering, Georgia Institute of Technology, Atlanta, GA 30332-0245, USA
[c]Metals and Ceramics Division, Oak Ridge National Laboratory, Oak Ridge, TN 37831-6064, USA

Received 1 August 2005; received in revised form 6 September 2005; accepted 9 September 2005
Available online 12 October 2005

Abstract

A series of compounds $\left(M^{III}_{0.5}M'^{V}_{0.5}\right)P_2O_7$, $M^{III}M'^{V}$ = AlTa, FeTa, GaTa, InNb, YNb, NdTa, and BiTa that are close structural relatives of cubic ZrP_2O_7 were prepared. Annealing samples with $M^{III}M'^{V}$ = InNb or YNb at temperatures above 600 °C did not lead to any long-range cation ordering. The thermal expansion characteristics of samples quenched from 1000 °C with $M^{III}M'^{V}$ = AlTa, InNb and YNb were investigated by high-temperature powder diffraction over the temperature range 25–600 °C. There are no lattice constant discontinuities in this range, unlike ZrP_2O_7. $(Al_{0.5}Ta_{0.5})P_2O_7$ and $(In_{0.5}Nb_{0.5})P_2O_7$ show linear coefficients of thermal expansion (CTEs) of $11.5(2)\times10^{-6}$ and $11.8(2)\times10^{-6}\,K^{-1}$, respectively. These values are similar to that for the low-temperature ZrP_2O_7 structure. However, the linear CTE for $(Y_{0.5}Nb_{0.5})P_2O_7$ ($4.8(2)\times10^{-6}\,K^{-1}$) is similar to that of the high-temperature form of ZrP_2O_7.

Keywords: Thermal expansion; Phase transition; Order–disorder

1. Introduction

Many compounds with structures related to that of ambient pressure ZrP_2O_7 [1–3] are known, as this framework can accommodate a very wide variety of cation sizes. Isostructural phosphates include $M^{IV}P_2O_7$ (Si, Ge, Sn, Pb, Zr, Hf, Ce, Pu, U, Th) [4–9] and some compounds containing transition metals in low oxidation states (ReP_2O_7 [10], WP_2O_7 [11], MoP_2O_7 [12], NbP_2O_7 [13], $Ta_{1-x}P_{1.8+x}O_7$ [14], $x\sim0.1$). The structure can be retained, in some cases, on substituting for the phosphorous with vanadium or arsenic, leading to ZrV_2O_7 [15], HfV_2O_7 [16], $ZrAs_2O_7$ and $HfAs_2O_7$ [17]. There has also been a report of compounds produced by replacing M^{IV} with mixed M^{III}/M^{V} cations leading to $Bi_{0.5}Ta_{0.5}P_2O_7$, $Bi_{0.5}Nb_{0.5}P_2O_7$, $Sb_{0.5}Ta_{0.5}P_2O_7$, $Nd_{0.5}Ta_{0.5}P_2O_7$ and $Eu_{0.5}Ta_{0.5}P_2O_7$ [14].

The structures of $M^{IV}P_2O_7$ have been under investigation since the work of Levi and Peyronel in 1935 [18]. They typically index quite well on a cubic subcell with ~8 Å dimensions. For the phosphates, the unit cell size varies in an almost linear fashion with the radius of the octahedral ion. At low temperature, nearly all of the materials show a superstructure. This often involves a $3\times3\times3$ enlargement of the basic cubic unit cell. In some cases, for example GeP_2O_7 [19], this superstructure is only approximately metrically cubic. Many of the compounds undergo a phase transition on heating that involves the loss of the superstructure. The exact nature of these superstructures is still an active area of investigation. However, its formation is driven by the desire to avoid linear P–O–P and V–O–V units. In the high-temperature cubic $\sim8\times8\times8$ Å unit cell, all the pyrophosphate and pyrovanadate groups are constrained by symmetry to have on average unfavorable 180° P–O–P and V–O–V bond angles. The $3\times3\times3$ enlargement of this basic unit cell in, for example, TiP_2O_7 and ZrV_2O_7 allows most, but not all, of these units to bend. Solid state NMR [2,19–23] has been used to confirm the space group symmetry of the superstructure and to distinguish between true 180° P–O–P/V–O–V/P–O–V units and static or dynamic disorder that leads to an average

*Corresponding author. Fax: +1 404 894 7452.
E-mail address: angus.wilkinson@chemistry.gatech.edu (A.P. Wilkinson).

0022-4596/$ - see front matter © 2005 Elsevier Inc. All rights reserved.
doi:10.1016/j.jssc.2005.09.006

180° bond angle. In some cases there is an intermediate incommensurate phase between the high-temperature and low-temperature forms [1,24].

Interest in the thermal expansion properties of compounds related to ZrP_2O_7 started in 1954 [25] after a report of a low-thermal-expansion material being formed in experiments examining the addition of P_2O_5 to ZrO_2 ceramic bodies [26]. Subsequently, the thermal expansion of GeP_2O_7 [19], TiP_2O_7 [27], ZrV_2O_7 [28,29], UP_2O_7 [30], ThP_2O_7 [31] and $Zr_{1-x}Th_xP_2O_7$ [32] were investigated. The 1995 publication of Korthuis et al. [33] discussing thermal expansion in the solid solution series $ZrV_{2-x}P_xO_7$ aroused additional interest in these materials. In TiP_2O_7 and GeP_2O_7 [19] the thermal expansion is positive at all reported temperatures. As materials with larger unit cells are examined, the behavior becomes more interesting. At low temperatures ZrP_2O_7 displays normal positive thermal expansion, but on transforming to its high-temperature structure (~290 °C) the thermal expansion coefficient becomes lower (see Fig. 1) [1]. Materials with larger unit cells, such as UP_2O_7, ThP_2O_7 and ZrV_2O_7, display negative thermal expansion at high temperature. Solid solution formation in the $ZrV_{2-x}P_xO_7$ system has been shown to suppress the structural phase transitions that are seen in the end members and for some compositions very low thermal expansion is observed over a wide temperature range [33].

In this paper, we report an initial examination of the thermal expansion characteristics of some $\left(\left(M^{III}_{0.5}M'^{V}_{0.5}\right)P_2O_7\right)$. In the work of Oyetola et al., (M^{III} = Sb, Bi, Nd, Eu and M^{V} = Sb, Nb, Ta) [14], some compounds of this type were prepared, but the thermal expansion and phase transitions of the products were not examined. As pointed out by Oyetola et al. [14], the $M^{III}M'^{V}$ ions in $\left(M^{III}_{0.5}M'^{V}_{0.5}\right)P_2O_7$ can, in principle, show well-defined long-range order or only the short-range order required for local charge balance. In general, it is expected that the presence of disorder on the octahedral cation sublattice in such a material will suppress the long-range ordering of the P_2O_7 units, that leads to supercell formation in ZrP_2O_7 and related materials, and stabilize the high-temperature low-thermal-expansion (P_2O_7 disordered) structure to lower temperatures. The possibility that the degree of cation ordering in $\left(M^{III}_{0.5}M'^{V}_{0.5}\right)P_2O_7$ materials can be manipulated by a judicious choice of heat treatment conditions was also of interest, as changing the extent of cation ordering offers a mechanism for both adjusting the thermal expansion properties and manipulating the phase transitions that are seen. A long-range-ordered arrangement of M^{III} and M^{V} is seen in β-$Sb^{III}Sb^{V}(P_2O_7)_2$. However, achieving an ordered state in such a material is easier than in a compound where M^{III} and M^{V} are different elements, as there is no need for cation migration, just electron migration. It is interesting to note that cation ordering in $\left(M^{III}_{0.5}M'^{V}_{0.5}\right)P_2O_7$ is formally analogous to the very well studied problem of ordering in 1:1 stoichiometry alloys with a face centered cubic (FCC) arrangement of metal sites, such as CuAu and CuPt [34]. The high-temperature form of ZrP_2O_7 belongs to space group *Pa*-3, but the zirconium sites are all symmetry equivalent and have a FCC arrangement. The M^{III} and M^{V} sites in β-$Sb^{III}Sb^{V}(P_2O_7)_2$ are ordered in an A_2B_2 pattern, which is different from that seen in CuAu or CuPt [34].

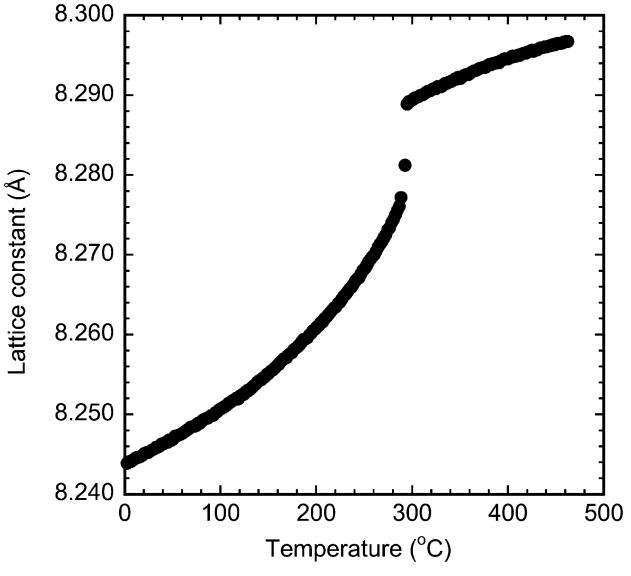

Fig. 1. Variation of lattice constants for ZrP_2O_7 as a function of temperature. Data were kindly supplied by J.S.O. Evans [1].

2. Experimental

2.1. Sample preparation

$\left(M^{III}_{0.5}M'^{V}_{0.5}\right)P_2O_7$ ($M^{III}M'^{V}$ = AlTa, FeTa, GaTa, InNb, YNb, NdTa): A M^{III} salt (usually a nitrate hydrate) was dissolved in the minimum amount of ethanol for complete dissolution (typically 4–5 mL/mmol of cation). An ethanolic solution of niobium or tantalum ethoxide containing 2,4-pentanedione (acetylacetone or acac) was also prepared (1:10:2 mole ratio metal:ethanol:acac). The M^{V}-pentaethoxide solution was added to the M^{III} solution while stirring. A stoichiometric amount of $(NH_4)_2HPO_4$, dissolved in the minimum amount of water, was then quickly added to the mixture. A gelatinous precipitate formed. A xerogel was obtained by drying at 100 °C overnight. The xerogel was decomposed by heating to 350 °C for 4 h. The resulting powder was fired at 1000 °C overnight.

$Bi_{0.5}Ta_{0.5}P_2O_7$: A slurry was made from the Ta-pentaethoxide:ethanol:acac (1:10:2) solution, crystalline $Bi(NO_3)_3 \cdot 5H_2O$ and concentrated (85%) phosphoric acid in a platinum crucible. It was stirred for 20 min, dried at 200 °C overnight and then heated at 700 °C for 12 h.

Several different heat treatments were employed. "Fast-cooled" samples were quenched by taking the crucibles out of the furnace and cooling to room temperature on the bench. A set of "Slow-cooled" samples were prepared by cooling in the furnace at a rate of ~1 °C/min. Portions of three samples were also annealed at 600, 700, 800 and 900 °C, respectively, in covered crucibles for 19 days. After annealing they were removed from the furnace and cooled to room temperature on the bench.

2.2. Diffraction data collection and analysis

Room-temperature X-ray diffraction patterns were recorded for all of the samples using a Scintag X1 diffractometer equipped with a Cu tube and Peltier-cooled solid state detector. Typically, they were recorded over the range 10–100° 2θ with a scan rate of 2°/min. These data were used for phase identification and the determination of room-temperature lattice constants.

Variable-temperature diffraction data were collected using two different sets of equipment. Data were collected in the range 25–600 °C for fast-cooled samples of $In_{0.5}Nb_{0.5}P_2O_7$ (15–75° 2θ) and $Y_{0.5}Nb_{0.5}P_2O_7$ (10–100° 2θ) using a PANalytical X'Pert PRO MPD X-ray diffractometer at the High Temperature Materials Laboratory (HTML), Oak Ridge National Laboratory, Oak Ridge, TN. These measurements employed copper K_α radiation, polycapillary optics on the incident beam side, a 0.09° parallel plate collimator with Soller slits on the diffracted beam side, a high count rate proportional detector (Miniprop), a scan rate of 1°/min, and an Anton-Paar XRK900 high-temperature stage. Additionally, diffraction data were collected in the range ~20–600 °C for fast-cooled samples of $Al_{0.5}Ta_{0.5}P_2O_7$ (10–100° 2θ), $In_{0.5}Nb_{0.5}P_2O_7$ (10–100° 2θ) and $Y_{0.5}Nb_{0.5}P_2O_7$ (10–100° 2θ) using a PANalytical X'Pert PRO MPD diffractometer at the Georgia Institute of Technology. These measurements made use of Cu K_α radiation, a parabolic mirror and 0.04 radian Soller slits on the incident beam side, a 0.09° parallel plate collimator on the diffracted beam side, a scan rate of 2°/min, a scintillation detector and an Anton-Paar HTK1200 high-temperature furnace. The temperature calibration of the later stage was checked using the phase transitions of $KClO_4$ and Ag_2SO_4 from ICTA (International Center for Thermal Analysis) standard set 759, and a correction was applied to the nominal sample temperatures based on these measurements.

Diffraction data analysis was carried out using JADE [35] for both qualitative phase analysis and lattice constant determination from the variable-temperature X-ray data. GSAS [36], with the EXPGUI interface [37], was used for the estimation of lattice constants from the room-temperature X-ray data.

2.3. Thermal analysis

Differential scanning calorimetery (DSC) measurements were performed using a Seiko 220. Temperature calibration was checked with the ICTA standard set 759. All DSC peaks were observed at temperatures within ±3 °C of the certified value, indicating that the instrument was well calibrated.

3. Results and discussion

Our syntheses, using niobium and tantalum ethoxides as starting materials, in general gave better quality samples than we were able to obtain using the previously reported method of Oyetola et al. [14], which made use of Ta_2O_5 or Nb_2O_5. However, many of the samples still contained impurity phases. The major phase in our samples of $Al_{0.5}Ta_{0.5}P_2O_7$, $Fe_{0.5}Ta_{0.5}P_2O_7$, $Ga_{0.5}Ta_{0.5}P_2O_7$, $In_{0.5}Nb_{0.5}P_2O_7$, $Y_{0.5}Nb_{0.5}P_2O_7$, $Nd_{0.5}Ta_{0.5}P_2O_7$ and $Bi_{0.5}Ta_{0.5}P_2O_7$ could be indexed on a cubic unit cell similar to that of ZrP_2O_7. The room-temperature unit cell constants for these materials are given in Table 1 along with the average ionic radius [38] for the $M^{III}M'^{V}$ cation pair. The lattice constants for all of these compounds, perhaps with the exception of $Bi_{0.5}Ta_{0.5}P_2O_7$, vary linearly with the average ionic radius as might be expected for a set of samples with the same structure and equivalent levels of disorder amongst the $M^{III}M'^{V}$ cation pairs (see Fig. 2). The variation of the room-temperature lattice constants for $\left(M^{III}_{0.5}M'^{V}_{0.5}\right)P_2O_7$ with average ionic radius is also in accord with the general trend in lattice constants seen for $M^{IV}P_2O_7$ phases (see Fig. 2), although the lattice constant for PbP_2O_7 [8,39] does not fit this trend well. The deviation of $Bi_{0.5}Ta_{0.5}P_2O_7$ from the above trends may in part be due to the presence of an s^2 pair of valence electrons in Bi^{3+}. The ionic radii in Shannon's compilation [38] assume some distortion of the coordination environment for such cations and, if there is less distortion in $Bi_{0.5}Ta_{0.5}P_2O_7$ than is typical for Bi^{3+}, this ionic radius estimate may be too large. In β-SbP_2O_7 [40], which has a ZrP_2O_7 related structure with an ordered arrangement of Sb^{III} and Sb^{V} cations, the coordination polyhedron for the Sb^{III} is highly distorted due to its s^2 valence pair and the metric symmetry is lower than cubic.

Table 1
The room temperature lattice constants for the fast cooled $\left(M^{III}_{0.5}M'^{V}_{0.5}\right)P_2O_7$ samples along with average $M^{III}M'^{V}$ cation radii [38] (six-coordinate values, high spin in the case of Fe)

Sample	Cation size (Å)	a (Å)
$Al_{0.5}Ta_{0.5}P_2O_7$	0.728	7.8863(5)
$Ga_{0.5}Ta_{0.5}P_2O_7$	0.770	7.9233(12)
$Fe_{0.5}Ta_{0.5}P_2O_7$	0.782	7.9807(3)
ZrP_2O_7	0.860	8.2416(2)
$In_{0.5}Nb_{0.5}P_2O_7$	0.860	8.0896(1)
$Y_{0.5}Nb_{0.5}P_2O_7$	0.910	8.2617(2)
$Nd_{0.5}Ta_{0.5}P_2O_7$	0.952	8.3047(5)
$Bi_{0.5}Ta_{0.5}P_2O_7$	0.975	8.2334(3)

A lattice constant for ZrP_2O_7 is given as a point of reference.

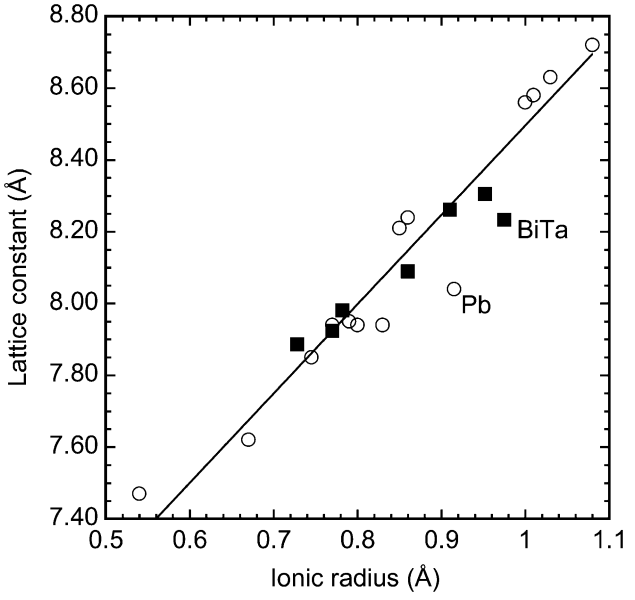

Fig. 2. Variation of the lattice constants for $M^{IV}P_2O_7$ (open circles) and $\left(M^{III}_{0.5}M'^{V}_{0.5}\right)P_2O_7$ (filled squares) as a function of cation or average cation radius.

In phases of the type $\left(M^{III}_{0.5}M'^{V}_{0.5}\right)P_2O_7$, the possibility of ordering amongst the M^{III} and M'^{V} cations should be considered. Ordering is likely to be primarily driven by electrostatic considerations and secondarily by strain relief. While there must be some short-range ordering of the cations to satisfy the requirement for local charge balance within the material, long-range order competes against the entropic benefits of having considerable disorder on the cation sublattice. In $A\left(M^{III}_{0.5}M'^{V}_{0.5}\right)O_3$ perovskites, such as $Pb(In_{0.5}Nb_{0.5})O_3$ [41–43] and $Pb(Sc_{0.5}Ta_{0.5})O_3$ [44–46], ordering amongst the cations on the *B* sublattice is strongly dependent on the sample's thermal history, with long-range ordering only developing on slow cooling or careful annealing. The driving force for cation ordering in $\left(M^{III}_{0.5}M'^{V}_{0.5}\right)P_2O_7$ phases, with the ZrP_2O_7 structure, is probably less than that for perovskites such as $PbIn_{0.5}Nb_{0.5}O_3$ and $PbSc_{0.5}Ta_{0.5}O_3$, as the metal ions, M^{III} and M'^{V}, are further apart from one another. Consequently, $\left(M^{III}_{0.5}M'^{V}_{0.5}\right)P_2O_7$ cooled rapidly from their synthesis temperatures are likely to have a disordered arrangement of cations.

Cation ordering in a material such as $\left(M^{III}_{0.5}M'^{V}_{0.5}\right)P_2O_7$ can reveal itself in diffraction patterns through the appearance of superlattice peaks and changes in lattice constants. We have chosen to primarily examine our samples for signs of cation ordering by monitoring their lattice constants, rather than by looking for superlattice reflections, as a function of heat treatment conditions. Lattice constants should be sensitive to changes in short and long-range ordering and are relatively easy to measure precisely. However, superlattice peaks could be missed as their positions depend upon the precise cation ordering pattern that is adopted, they will be broad unless the ordered domain size is quite large, and for many of the compositions of interest there is little X-ray scattering contrast between the M^{III} and M'^{V} ions.

Samples of $Al_{0.5}Ta_{0.5}P_2O_7$, $In_{0.5}Nb_{0.5}P_2O_7$ and $Y_{0.5}Nb_{0.5}P_2O_7$ were subjected to a series of different heat treatments to examine the effect, if any, of thermal history on cation ordering in these materials. Prolonged annealing led to the degradation of the $Al_{0.5}Ta_{0.5}P_2O_7$ samples and some decomposition was also observed in samples of $Y_{0.5}Nb_{0.5}P_2O_7$ heated at higher temperatures. This decomposition was probably associated with the evaporation of P_2O_5. Lattice constants were determined for samples of $In_{0.5}Nb_{0.5}P_2O_7$ annealed for 19 days at 600, 700, 800 and 900 °C and for samples of $Y_{0.5}Nb_{0.5}P_2O_7$ that had been annealed for 19 days at 600, 700, and 800 °C. Within experimental error, the room-temperature lattice constants for these annealed samples were identical to one another and to those of samples prepared by rapid cooling from 1000 °C after initial synthesis. This indicates that annealing at or above 600 °C does not induce any cation ordering in the compositions examined. In a separate series of experiments, several batches of $In_{0.5}Nb_{0.5}P_2O_7$ and $Y_{0.5}Nb_{0.5}P_2O_7$ were slow cooled (~1 °C/min) from 1000 °C and their lattice constants compared with those for samples that were quenched from 1000 °C. The lattice constants for the slow-cooled samples were observed to be consistently slightly smaller (~0.01 Å) than those for the quenched samples. Other than for the shifts in the peak positions, there were no obvious differences between the diffraction patterns of the slow-cooled and quenched samples. These observations suggest that at <600 °C some, probably short-range, cation ordering may be taking place.

ZrP_2O_7 shows a pronounced endotherm, by DSC, on heating to ~290 °C due to the well-known order–disorder transition associated with the loss of its $3\times3\times3$ superlattice [1,3] at this temperature. Fast-cooled samples of $In_{0.5}Nb_{0.5}P_2O_7$ and $Y_{0.5}Nb_{0.5}P_2O_7$ were examined by DSC to see if there was a similar endotherm. These compounds were chosen because they were well crystallized and of good purity, although there was some evidence of $InPO_4$ and $NbPO_5$ in the indium phase and an unidentified impurity in the yttrium phase. There was no evidence in the DSC measurements for any transition between room temperature and 500 °C.

Fast-cooled samples of $In_{0.5}Nb_{0.5}P_2O_7$, $Y_{0.5}Nb_{0.5}P_2O_7$ and $Al_{0.5}Ta_{0.5}P_2O_7$ were examined by variable-temperature powder diffraction to look for signs of an order–disorder transition like that observed in ZrP_2O_7 at ~290 °C, and to examine their thermal expansion characteristics. Unlike the yttrium and indium samples, the $Al_{0.5}Ta_{0.5}P_2O_7$ showed considerable peak broadening leading to lower-quality diffraction patterns than those for the other two phases

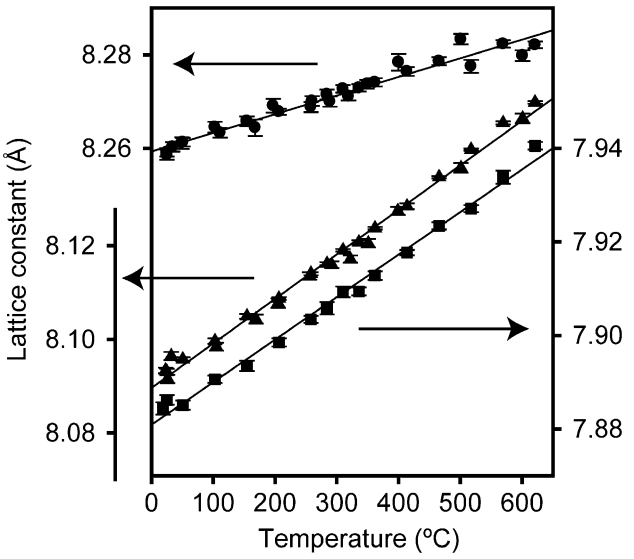

Fig. 3. Lattice constants as a function of temperature for $Al_{0.5}Ta_{0.5}P_2O_7$ (squares), $In_{0.5}Nb_{0.5}P_2O_7$ (triangles) and $Y_{0.5}Nb_{0.5}P_2O_7$ (circles). Error bars on the data points are one standard deviation. Straight-line best fits to the data are also shown.

measured under similar conditions. This phase also contained some $AlPO_4$ and $TaPO_5$ impurities.

Lattice constants were refined by fitting individual peak positions using JADE (v 6.5) for both the data obtained from GTECH and ORNL. We graphically present the lattice constants as a function of temperature for these three compounds including data from both sources in Fig. 3 (the lattice constants are available as Supplementary Material). Linear coefficients of thermal expansion (CTEs) for these compounds and ZrP_2O_7 were estimated by straight-line fits to the data. The resulting average CTEs are summarized in Table 2. The lattice constants for the $\left(M^{III}_{0.5}M'^{V}_{0.5}\right)P_2O_7$ compounds show no sign of a discontinuity like that seen for ZrP_2O_7 at ~290 °C (see Fig. 1). This implies that a transition similar to that in ZrP_2O_7 does not occur for these compounds or that it occurs outside the measured temperature range. It is interesting to note that the CTEs for $Al_{0.5}Ta_{0.5}P_2O_7$ ($11.5(2)\times10^{-6}\,K^{-1}$) and $In_{0.5}Nb_{0.5}P_2O_7$ ($11.8(2)\times10^{-6}\,K^{-1}$), over the range 25–620 °C, are similar to one another and close to the value estimated for ZrP_2O_7 ($12.4(1)\times10^{-6}\,K^{-1}$), in the range 25–260 °C (below its phase transition), but the CTE for $Y_{0.5}Nb_{0.5}P_2O_7$ ($4.8(2)\times10^{-6}\,K^{-1}$) over the range 25–620 °C is very similar to that for ZrP_2O_7 ($4.20(7)\times10^{-6}\,K^{-1}$), at high temperature (400–463 °C).

The CTEs for the examined $\left(M^{III}_{0.5}M'^{V}_{0.5}\right)P_2O_7$ phases do not show a smooth trend with average ionic radius for $M^{III}M'^{V}$. The values for $Al_{0.5}Ta_{0.5}P_2O_7$ and $In_{0.5}Nb_{0.5}P_2O_7$ are similar even though the average ionic radii differ by ~18%, but on going to $Y_{0.5}Nb_{0.5}P_2O_7$ where the average ionic radius is only ~6% larger than that for $In_{0.5}Nb_{0.5}P_2O_7$, the CTE drops dramatically. These observations, along with those in the previous paragraph, may indicate that $Y_{0.5}Nb_{0.5}P_2O_7$ has a structure similar to that of the high-temperature form of ZrP_2O_7, but the other two phases may have structures similar to that of the low-temperature form of ZrP_2O_7. The room-temperature lattice constant of $Y_{0.5}Nb_{0.5}P_2O_7$ (8.26 Å) is very similar to that of ZrP_2O_7 (8.24 Å) suggesting that the disorder introduced by replacing Zr with $Y_{0.5}Nb_{0.5}$ is enough to stabilize the high-temperature low-thermal-expansion ZrP_2O_7 structure to below room temperature. The adoption of the low-temperature ZrP_2O_7 structure by $Al_{0.5}Ta_{0.5}P_2O_7$ is perhaps not surprising as TiP_2O_7 has a very similar lattice constant to $Al_{0.5}Ta_{0.5}P_2O_7$ and it does not transform to the high-temperature structure below 1000 °C [19,27]. The available laboratory X-ray data for $Al_{0.5}Ta_{0.5}P_2O_7$ and $In_{0.5}Nb_{0.5}P_2O_7$ do not show clear signs of extra peaks from a $3\times3\times3$ superlattice like that found in the low-temperature form of ZrP_2O_7. However, the quality of the data, including the presence of impurity peaks and the low crystallinity of the $Al_{0.5}Ta_{0.5}P_2O_7$ sample, do not allow a definitive conclusion to be made.

Table 2
Comparison of thermal expansion coefficients for $Al_{0.5}Ta_{0.5}P_2O_7$, $In_{0.5}Nb_{0.5}P_2O_7$, $Y_{0.5}Nb_{0.5}P_2O_7$ and ZrP_2O_7

Compound and temperature range	α ($10^{-6}\,K^{-1}$)
$AlTaP_4O_{14}$ up to 620 °C	11.5(2)
$InNbP_4O_{14}$ up to 620 °C	11.8(2)
$YNbP_4O_{14}$ up to 620 °C	4.8(2)
ZrP_2O_7 25–260 °C	12.4(1)[a]
ZrP_2O_7 400–463 °C	4.20(7)[a]

[a]Values derived from a linear fit to lattice constants supplied by J.S.O. Evans [1].

4. Conclusions

The replacement of zirconium in ZrP_2O_7 by a mixture of M^{III} and M'^{V} cations, with an average ionic radius similar to that of Zr^{IV}, produces compounds of the type $\left(M^{III}_{0.5}M'^{V}_{0.5}\right)P_2O_7$ that are structural relatives of cubic ZrP_2O_7. Samples quenched from 1000 °C show no signs, in the temperature range 25–600 °C, of the order–disorder phase transition that is seen in ZrP_2O_7 at ~290 °C and no evidence of any long-range cation ($M^{III}M'^{V}$) ordering. The thermal expansion coefficients of $Al_{0.5}Ta_{0.5}P_2O_7$ and $In_{0.5}Nb_{0.5}P_2O_7$ are similar to that of the low-temperature form of ZrP_2O_7 but the CTE for $Y_{0.5}Nb_{0.5}P_2O_7$ is much lower and similar to that of the high-temperature form of ZrP_2O_7. Further work examining a wider range of compounds, and a wider range of temperatures is needed to fully understand how the replacement of Zr in the cubic ZrP_2O_7 structure by $M^{III}_{0.5}M'^{V}_{0.5}$ affects the thermophysical properties of the products.

Acknowledgments

This research was supported by National Science Foundation grant DMR-0203342. Some of the XRD data were collected at the Diffraction User Center, Oak Ridge National Laboratory, sponsored by the Assistant Secretary for Energy Efficiency and Renewable Energy, Office of Transportation Technologies, as part of the High Temperature Materials Laboratory User Program, Oak Ridge National Laboratory, managed by UT-Battelle, LLC, for the US Dept. of Energy under contract DE-AC05-00OR22725. We are grateful to the reviewers for insightful comments.

Appendix A. Supplementary Materials

Supplementary data associated with this article can be found in the online version at doi:10.1016/j.jssc.2005.09.006.

References

[1] R.L. Withers, Y. Tabira, J.S.O. Evans, I.J. King, A.W. Sleight, J. Solid State Chem. 157 (2001) 186–192.
[2] I.J. King, F. Fayon, D. Massiot, R.K. Harris, J.S.O. Evans, Chem. Commun. (2001) 1766–1767.
[3] N. Khosrovani, V. Korthuis, A.W. Sleight, T. Vogt, Inorg. Chem. 35 (1996) 485–489.
[4] C.W. Bjorklund, J. Am. Chem. Soc. 79 (1958) 6347–6350.
[5] L.-O. Hagman, P. Kierkegaard, Acta Chem. Scand. 23 (1969) 327–328.
[6] V.F. Liebau, G. Bissert, N. Koppen, Z. Anorg. Allg. Chem. 359 (1968) 113–134.
[7] C.-H. Huang, O. Knop, D.A. Othen, Can. J. Chem. 53 (1975) 79–91.
[8] H. Vollenkle, A. Wittmann, H. Nowotny, Monatshefte Chem. 94 (1963) 956–963.
[9] A. Burdese, M. Lucco Borlera, Ann. Chim. (Rome) 53 (1963) 333–343.
[10] E. Banks, R. Sacks, Mater. Res. Bull. 17 (1982) 1053–1055.
[11] Z.S. Teweldemedhin, K.V. Ramanujachary, M. Greenblatt, Mater. Res. Bull. 28 (1993) 427–434.
[12] N. Kinomura, M. Hirose, N. Kumada, F. Muto, Mater. Res. Bull. 20 (1985) 379–382.
[13] J.J. Zah-Letho, S. Oyetola, A. Verbaere, F. Tauelle, Y. Piffard, Eur. J. Solid State Chem. 31 (1994) 1009–1020.
[14] S. Oyetola, A. Verbaere, D. Guyomard, M.P. Crosnier, Y. Piffard, M. Tournoux, Eur. J. Solid State Inorg. Chem. 28 (1991) 23–36.
[15] J.S.O. Evans, J.C. Hanson, A.W. Sleight, Acta Crystallogr. B 54 (1998) 705–713.
[16] E.J. Baran, J. Less Common Methods 46 (1976) 343–345.
[17] H. Onken, Die Naturwissenschaften 52 (1965) 344.
[18] G.R. Levi, G. Peyronel, Z. Kristallogr. 92 (1935) 190–209.
[19] E.R. Losilla, A. Cabeza, S. Bruque, M.A.G. Aranda, J. Sanz, J.E. Iglesias, J.A. Alonso, J. Solid State Chem. 156 (2001) 213–219.
[20] J. Sanz, J.E. Iglesias, J. Soria, E.R. Losilla, M.A.G. Aranda, S. Bruque, Chem. Mater. 9 (1997) 996–1003.
[21] C. Hudalla, H. Eckert, R. Dupree, J. Phys. Chem. 100 (1996) 15986–15991.
[22] R.J. Iuliucci, B.H. Meier, J. Am. Chem. Soc. 120 (1998) 9059–9062.
[23] X. Helluy, C. Marichal, A. Sebald, J. Phys. Chem. B 104 (2000) 2836–2845.
[24] R.L. Withers, J.S.O. Evans, J. Hanson, A.W. Sleight, J. Solid State Chem. 137 (1998) 161–167.
[25] D.E. Harrison, H.A. McKinstry, F.A. Hummel, J. Am. Ceram. Soc. 37 (1954) 277–280.
[26] G.R. Pole, A.W. Beinlich, N. Gilbert, J. Am. Ceram. Soc. 29 (1946) 208–222.
[27] D.E. Harrison, F.A. Hummel, J. Am. Ceram. Soc. 42 (1959) 487–490.
[28] R.C. Buchanan, G.W. Walter, J. Electrochem. Soc. 130 (1983) 1905–1910.
[29] D.F. Craig, F.A. Hummel, J. Am. Ceram. Soc. 55 (1972) 532.
[30] H.P. Kirchner, K.M. Merz, W.R. Brown, J. Am. Ceram. Soc. 46 (1963) 137–141.
[31] K. Laud, F.A. Hummel, J. Am. Ceram. Soc. 54 (1971) 296–298.
[32] K.R. Laud, F.A. Hummel, J. Am. Ceram. Soc. 54 (1971) 407–409.
[33] V. Korthuis, N. Khosrovani, A.W. Sleight, N. Roberts, R. Dupree, W.W. Warren, Chem. Mater. 7 (1995) 412–417.
[34] F. Ducastelle, Order and Phase Stability in Alloys, North-Holland, Amsterdam, 1991.
[35] Computer program JADE, Materials Data, Inc., Livermore, CA, 1995–2005.
[36] A.C. Larson, R.B. Von Dreele, GSAS—General Structure Analysis System Report LA-UR-86-748, Los Alamos Laboratory, 1987.
[37] B.H. Toby, J. Appl. Crystallogr. 34 (2001) 210–213.
[38] R.D. Shannon, Acta Crystallogr. A 32 (1976) 751–767.
[39] P. Giorgio, Gaz. Chim. Ital. 69 (1939) 254–262.
[40] A. Verbaere, S. Oyetola, D. Guyomard, Y. Piffard, J. Solid State Chem. 75 (1988) 217–224.
[41] P. Groves, J. Phys. C: Solid State Phys. 19 (1986) 111–128.
[42] P. Groves, J. Phys. C: Solid State Phys. 19 (1986) 5103–5120.
[43] A.A. Bokov, I.P. Rayevskii, V.G. Smotrakov, O.I. Prokopalo, Phys. Status Solidi (a) 93 (1986) 411–417.
[44] M.P. Harmer, J. Chen, P. Peng, H.M. Chan, D.M. Smyth, Ferroelectrics 97 (1989) 263–273.
[45] N. Setter, L.E. Cross, J. Mater. Sci. 15 (1980) 2478–2482.
[46] N. Setter, L.E. Cross, J. Appl. Phys. 51 (1980) 4356–4360.